Target mass corrections and higher twist effects in polarized deep-inelastic scattering

S. Taheri Monfared,[1,*] Z. Haddadi,[2,†] and Ali N. Khorramian[3,1,‡]

[1]*School of Particles and Accelerators, Institute for Research in Fundamental Sciences (IPM), P.O. Box 19395-5531 Tehran, Iran*

[2]*KVI/University of Groningen, 9747 AA Groningen, Netherlands*

[3]*Physics Department, Semnan University, 35131-19111 Semnan, Iran*

(Received 13 December 2013; published 30 April 2014; publisher error corrected 28 May 2014)

We perform a next-to-leading-order QCD analysis to world data on polarized structure functions g_1 and g_2 in a fixed-flavor number scheme. We include target mass corrections and higher twist effects in our fitting procedure and study their non-negligible effects on physically interesting quantities. Twist-3 contributions to both polarized structure functions are determined, and the accuracy of the extracted polarized parton distribution functions is improved. ^{3}He and ^{3}H polarized structure functions are described based on our fit result. Moreover, sum rules are derived and compared with available theoretical and experimental results.

DOI: 10.1103/PhysRevD.89.074052 PACS numbers: 13.60.Hb, 12.39.-x, 14.65.Bt

I. INTRODUCTION

The determination of the nucleon's spin into its quark and gluon components is still an important challenge in particle physics. The deep-inelastic scattering (DIS) experiments performed at DESY, SLAC, CERN, and JLAB have refined our understanding of the spin distributions and revealed the spin-dependent structure functions of the nucleon. The polarized structure functions $g_1(x, Q^2)$ and $g_2(x, Q^2)$ are measured in deep-inelastic scattering of a longitudinally polarized lepton on polarized nuclear targets.

Theoretical models have remarkably improved since the early framework of quark parton model (QPM) indicated that g_1 measures only quark contributions to the nucleon's spin and g_2 is identically zero. Afterward, perturbative quantum chromodynamics (pQCD) analysis in the next-to-leading-order (NLO) approximation provides information on the role of gluons in the overall spin of the nucleon. Moreover, g_2 contains nonperturative higher twist (HT) contributions, such as quark-quark and quark-gluon correlations and quark mass effects, which are not interpreted in QPM. Operator Product Expansion (OPE) based on QCD is an appropriate formalism that is applicable to interpret g_2 structure function [1,2].

The traditional method to perform global fits concentrates on the extraction of leading twist parton distribution functions (PDFs), using cuts on minimum values of Q^2 and hadronic final-state mass squared W^2. The cuts are of the order $Q^2 \gtrsim 4$ GeV^2 and $W^2 \gtrsim 14$ GeV^2 [3,4], which means that x is limited to $x \lesssim 0.7$. These kinematic cuts eliminate the contribution of corrections from various nonperturbative effects at finite Q^2, such as target mass corrections (TMCs) [5] and dynamical higher twist contributions [6]. These corrections become increasingly significant as Q^2 is reduced and x tends to 1. The large-x behavior of PDFs is extrapolated in this classical scenario.

Extraction of polarized PDFs (PPDFs) from a variety of experiments within NLO analyses is an important phenomenological issue [7–15]. To compensate for the scarcity of polarized high-energy data points available to global polarized PDF analyses, the applied cuts were relaxed; thereby, one is typically forced to make use of the data at lower Q^2 and higher x. Consequently, pQCD calculation cannot be trusted alone. As will be shown subsequently, in this kinematical region ($Q^2 \sim 1 - 5$ GeV^2, 4 GeV$^2 <$ W$^2 < 10$ GeV^2), TMCs and HT contributions are important. Some of the existing studies, such as Refs. [8,9,11,16–18], use these effects in their global fitting procedure. Note that the g_2 polarized structure function is not considered in these analyses. But it helps to determine the low-Q^2 corrections due to following reasons. First, leading and higher twist contributions appear with the same order of importance. Second, g_2 data are mostly in the low-Q^2 region in which the effects of TMCs and HT become significant. Because of the mentioned points, we believe that, although data for spin structure function g_2 is not accurate enough, at the current level of accuracy, analyzing both g_1 and g_2 structure functions provides a fertile ground to study the mentioned effects. A future high-luminosity machine, like the electron-ion collider, is required to study the twist-3 contributions in detail [19].

In our latest analysis [14], we determined PPDFs based on Jacobi polynomials using only g_1 experimental data and simply considered $g_1(x, Q^2) = g_1(x, Q^2)_{\mathrm{pQCD}}$. In the present study, we improve our precision with full g_1 and g_2

*Sara.taheri@ipm.ir
†z.haddadi@rug.nl
‡Khorramiana@theory.ipm.ac.ir

analysis including TMCs and HT contributions. No polynomial technique is adopted.

The outline of the paper is as follows. We give an introduction to the theoretical framework that describes polarized structure functions in Sec. II. Section III provides detailed information about our QCD analysis. A discussion of fit results is given in Sec. IV. In Sec. V, we compute the nuclear structure functions, and in Sec. VI, we check various polarized sum rules. Section VII contains the concluding remarks.

II. THEORETICAL ANALYSIS

In the QCD polarized structure function, g_1 consists of two parts, the leading twist (LT) ($\tau = 2$) and the higher twist ($\tau \geq 3$) contributions:

$$g_1(x,Q^2) = g_1(x,Q^2)_{\mathrm{LT}} + g_1(x,Q^2)_{\mathrm{HT}}. \tag{1}$$

The LT term can be determined from

$$g_1(x,Q^2)_{\mathrm{LT}} = g_1(x,Q^2)_{\mathrm{pQCD}} + h^{\mathrm{TMCs}}(x,Q^2)/Q^2 + \mathcal{O}(M^4/Q^4). \tag{2}$$

$g_1(x,Q^2)_{\mathrm{pQCD}}$ is achievable via NLO perturbative QCD when the nucleon mass is put equal to zero and h^{TMCs} is calculable in pQCD. It is kinematic in origin and contains terms suppressed by powers of M^2/Q^2 at large values of Q^2.

The contribution of multiparton correlation in the nucleon is considered through the dynamical higher twist terms

$$g_1(x,Q^2)_{\mathrm{HT}} = h(x,Q^2)/Q^2 + \mathcal{O}(\Lambda^4/Q^4), \tag{3}$$

where $h(x,Q^2)$ are nonpurtubative effects that can be calculated in a model-dependent manner. They are dynamical in origin and suppressed by powers of Λ^2/Q^2. Λ is the scale of nonperturbative parton-parton correlation. These corrections become increasingly important at the low-energy scale.

The spin-structure function g_2 does not have a direct interpretation in pQCD. It can be understood using the OPE in which g_2 is separated into [20]

$$g_2(x,Q^2) = g_2^{WW}(x,Q^2) + \bar{g}_2(x,Q^2). \tag{4}$$

Here, $g_2^{WW}(x,Q^2)$ is a twist-2 part, and

$$\bar{g}_2(x,Q^2) = -\int_x^1 \frac{\partial}{\partial y}\left[\frac{m_q}{M}h_T(y,Q^2) + \zeta(y,Q^2)\right]\frac{dy}{y}. \tag{5}$$

The twist-3 part, $\zeta(y,Q^2)$, arises from nonperturbative multiparton interaction, which will be discussed in the next section. h_T depends on the quark transverse polarization density in twist-2, which is suppressed by the ratio of the quark to nucleon masses $\frac{m_q}{M}$. Consequently, any deviation of g_2 from g_2^{WW} is from the twist-3 contribution. It is in special properties of g_2 that its HT contribution can be equally important as its twist-2 part, since it is not suppressed by inverse powers of Q^2.

A. Leading twist

The leading twist contributions to the $g_1(x,Q^2)$ for the proton and neutron are available in the NLO [21] by

$$g_1(x,Q^2)_{\mathrm{pQCD}} = \frac{1}{2}\sum_q^{n_f} e_q^2\left\{[\delta q + \delta\bar{q}] \otimes \left(1 + \frac{\alpha_s}{2\pi}\delta C_q\right) + \frac{\alpha_s}{2\pi}\delta g \otimes \frac{\delta C_g}{n_f}\right\}. \tag{6}$$

Here, typical convolution in x space is represented with the symbol $\otimes$. δq, $\delta\bar{q}$, and δg are polarized quark, antiquark, and gluon densities, which are evolved to Q^2 with the solution of Dokshitzer-Gribov-Lipatov-Alterelli-Parisi (DGLAP) evolution equations in Mellin space. $\delta C_{q,g}$ are Wilson coefficient functions in NLO. The deuteron structure function can be obtained via the relation

$$g_1^d(x,Q^2)_{\mathrm{pQCD}} = \frac{1}{2}\{g_1^p(x,Q^2)_{\mathrm{pQCD}} + g_1^n(x,Q^2)_{\mathrm{pQCD}}\} \times (1 - 1.5w_D), \tag{7}$$

from proton and neutron ones, where $w_D = 0.05 \pm 0.01$ is the probability to find the deuteron in a D state.

Because of the fact that g_1 and g_2 contain the same twist-2 operators, the leading twist part of g_2 can be extracted via the Wandzura–Wilczek (WW) relation [22,23]

$$g_2^{WW}(x,Q^2)_{\mathrm{pQCD}} = -g_1^p(x,Q^2)_{\mathrm{pQCD}} + \int_x^1 \frac{dy}{y} g_1^p(y,Q^2)_{\mathrm{pQCD}}. \tag{8}$$

This relation remains valid when target mass corrections are included in the twist-2 contribution [23,24].

B. Target mass corrections and threshold problem

To perform a reliable fit that contains data at lower values of Q^2, nucleon mass corrections cannot be neglected. We follow the method suggested by Refs. [23,25,26], which is exactly calculable and effectively belongs to the LT term [27].

There is a traditional challenge with the behavior of the both polarized and unpolarized target mass corrected structure functions in the neighborhood of $x = 1$. Many attempts have been made to avoid this issue by considering various prescriptions in the literature [5,23,28–31]. These solutions are not unique. In this paper, we follow the prescription of Ref. [32] to avoid the threshold problem in

the polarized structure function. D'Alesio *et al.* [32] impose the simplest probability for hadronization $\theta(x_{TH}-x)$. Here, the largest kinematically accepted amount of x for inelastic scattering is x_{TH}, which is defined as

$$x_{TH}=\frac{Q^2}{Q^2+\mu(2M+\mu)}, \tag{9}$$

where μ should be the lowest mass particle that can be produced in the process of interest. We modified our polarized structure functions by multiplying them into the θ function.

C. Higher twist

Higher twist terms arising from long-range nonperturbative multiparton correlations contribute at low values of Q^2. The Braun-Lautenschlager-Manashov-Pirnay (BLMP) model [33] made a step in developing a usable parametrization for phenomenological analysis. It constructed HT distributions from convolution integrals of the light-cone wave functions by considering a simple model based on three valence quarks and one gluon with the total zero angular momentum.

Accordingly, we applied the parametrization form suggested by the BLMP model,

$$\begin{aligned} g_2^{tw-3}(x) = A[\ln(x)+(1-x)+\frac{1}{2}(1-x)^2] \\ +(1-x)^3[B-C(1-x)+D(1-x)^2 \\ -E(1-x)^3], \end{aligned} \tag{10}$$

in our initial scale and fit the coefficients to the data. We applied a nonsinglet evolution equation, since higher twist contributions are specially important in large-x values. This approach is compared with exact evolution equations for the gluon-quark-antiquark correlation in Ref. [33]. They are practically equal.

By the integral relation of

$$\begin{aligned} g_1^{tw-3}(x,Q^2) = \frac{4x^2M^2}{Q^2}\left[g_2^{tw-3}(x,Q^2)\right. \\ \left.-2\int_x^1\frac{dy}{y}g_2^{tw-3}(y,Q^2)\right], \end{aligned} \tag{11}$$

the twist-3 part of different spin-dependent structure functions, g_1^{tw-3} and g_2^{tw-3}, are related [25].

III. QCD ANALYSIS AND FITTING PROCEDURE

A. Parametrization

We have adopted the following parametrization at the initial scale of $Q_0^2=4$ GeV^2 for $q=\{u_v,d_v,\bar{q},g\}$:

$$x\delta q(x,Q_0^2)=\mathcal{N}_q\eta_q x^{a_q}(1-x)^{b_q}(1+c_q x). \tag{12}$$

The normalization constants $\mathcal{N}_q$,

$$\mathcal{N}_q^{-1}=\left(1+c_q\frac{a_q}{a_q+b_q+1}\right)B(a_q,b_q+1), \tag{13}$$

are selected such that η_q are the first moments of the PPDFs. $B(a,b)$ is the Euler beta function. Considering SU(3) flavor symmetry, we have $\delta\bar{q}\equiv\delta\bar{u}=\delta\bar{d}=\delta s=\delta\bar{s}$.

The free unknown parameters provide a fit with a large degree of flexibility. Some of our input parameters are subjected to constraints due to following reasons:

(i) The first moments of the polarized valence quark densities can be related to F and D as measured in neutron and hyperon β decays [34]. These constraints lead to the values of $\eta_{u_v}=0.928\pm0.014$ and $\eta_{d_v}=-0.342\pm0.018$.

(ii) $c_{\bar{q}}$ and c_g are set to zero due to the present accuracy of the data. No improvement is observed in the fit with nonzero values of them.

(iii) The $b_{\bar{q}}$ and b_g parameters, which control the large-x behavior of the polarized sea quarks and gluons, have large uncertainties in a region that is dominated by the valence distribution. We fixed them with the ratio of $b_{\bar{q}}/b_g\sim1.6$, which is derived from the analogous unpolarized parameters.

The rest of parameters $\{A,B,C,D,E\}$ are the unknown higher twist parameters for to $g_{2,\{p,n,d\}}$ and consequently $g_{1,\{p,n,d\}}$. They are determined from a simultaneous fit to the all polarized structure function data of g_1 and g_2.

The parameters $\{\eta_{u_v},\eta_{d_v},c_{\bar{q}},c_g\}$ and the ratio of b values are frozen in the first minimization procedure. In the second minimization, we fix $\{b_{\bar{q}},b_g,c_{u_v},c_{d_v}\}$ and $\{A,B,C,D,E\}$ as demonstrated in Tables I and II. There are potentially nine unknown parameters in the fit, including $\alpha_s(Q_0^2)$, which provide enough flexibility to have a reliable fit.

TABLE I. Final parameter values and their statistical errors at the input scale $Q_0^2=4$ GeV^2 determined from two different global analyses. Those marked with (*) are fixed.

Parameters		Full scenario	pQCD scenario
δu_v	η_{u_v}	0.928^*	0.928^*
	a_{u_v}	0.558 ± 0.012	0.619 ± 0.018
	b_{u_v}	3.460 ± 0.006	3.234 ± 0.077
	c_{u_v}	8.848^*	5.468^*
δd_v	η_{d_v}	-0.342^*	-0.342^*
	a_{d_v}	0.250 ± 0.033	0.226 ± 0.042
	b_{d_v}	3.912 ± 0.116	3.822 ± 0.357
	c_{d_v}	14.162^*	25.09^*
$\delta_{\bar{q}}$	$\eta_{\bar{q}}$	-0.0605 ± 0.006	-0.0565 ± 0.022
	$a_{\bar{q}}$	0.567 ± 0.009	0.597 ± 0.075
	$b_{\bar{q}}$	4.993^*	7.355^*
	$c_{\bar{q}}$	0.0^*	0.0^*
δg	η_g	0.201 ± 0.044	0.147 ± 0.054
	a_g	2.253 ± 0.010	3.177 ± 0.58
	b_g	3.082^*	4.540^*
	c_g	0.0^*	0.0^*
$\alpha_s(Q_0^2)$		0.365 ± 0.011	0.362 ± 0.016
χ^2/ndf		$405.38/508=0.798$	$559.6/508=1.101$

TABLE II. Parameter values for the coefficients of the twist-3 corrections at $Q^2 = 4$ GeV^2 obtained in the full scenario.

	A	B	C	D	E
$g_{2,p}^{tw-3}$	0.034	0.554	−0.387	−1.17	0.969
$g_{2,n}^{tw-3}$	0.067	0.106	−0.448	0.569	−0.098
$g_{2,d}^{tw-3}$	0.307	0.117	−0.210	0.657	−0.083

B. Overview of data sets

We use a wide range of polarized deep-inelastic scattering lepton-nucleon data on spin structure functions g_1 [2,35–49] and g_2 [2,35,45,48–52], which are extracted based on the different nucleon targets of protons, neutrons, and deuterons to extract all PPDFs.

The major properties of these data sets are summarized in Table III, which contains the name of the experimental group, the covered kinematic ranges in x and Q^2, the number of available data points, and the fitted normalization shifts $\mathcal{N}_i$. Our analysis is limited to the region of $Q^2 \geq 1$ GeV^2, to ensure that perturbative QCD is applicable, and $W^2 \geq 3$ GeV^2. The cut on W^2 is slightly smaller than in some previous PPDF analyses.

Although most of the g_2 data have large errors, we considered them in the fitting procedure. Thus, our results focus on the quality or characteristic of the twist-3 part rather than on their quantity.

TABLE III. Published data points above $Q^2 = 1.0$ GeV^2. Each experiment is given the x and Q^2 ranges, the number of data points for each given target, and the fitted normalization shifts $\mathcal{N}_i$ (see the text).

Experiment	Ref.	x range	Q^2 range (GeV^2)	Number of data points	$\mathcal{N}_n$
E143(p)	[35]	0.031–0.749	1.27–9.52	28	0.9999
HERMES(p)	[36]	0.028–0.66	1.01–7.36	39	1.0011
SMC(p)	[37]	0.005–0.480	1.30–58.0	12	0.9998
EMC(p)	[38]	0.015–0.466	3.50–29.5	10	1.0050
E155	[39]	0.015–0.750	1.22–34.72	24	1.0189
HERMES06(p)	[40]	0.026–0.731	1.12–14.29	51	0.9990
COMPASS10(p)	[41]	0.005–0.568	1.10–62.10	15	0.9904
g_1^p				**179**	
E143(d)	[35]	0.031–0.749	1.27–9.52	28	0.9998
E155(d)	[42]	0.015–0.750	1.22–34.79	24	1.0001
SMC(d)	[37]	0.005–0.479	1.30–54.80	12	1.0000
HERMES06(d)	[40]	0.026–0.731	1.12–14.29	51	0.9992
Compass05(d)	[43]	0.0051–0.4740	1.18–47.5	11	0.9980
Compass06(d)	[44]	0.0046–0.566	1.10–55.3	15	1.0000
g_1^d				**141**	
E142(n)	[45]	0.035–0.466	1.10–5.50	8	0.9990
HERMES(n)	[36]	0.033–0.464	1.22–5.25	9	1.0000
E154(n)	[46]	0.017–0.564	1.20–15.00	17	0.9995
HERMES06(n)	[47]	0.026–0.731	1.12–14.29	51	1.0000
Jlab03(n)	[49]	0.14–0.22	1.09–1.46	4	1.0001
Jlab04(n)	[48]	0.33–0.60	2.71–4.8	3	1.0996
Jlab05(n)	[2]	0.19–0.20	1.13–1.34	2	1.0353
g_1^n				**94**	
E143(p	[35]	0.038–0.595	1.49–8.85	12	0.9999
E155(p	[50]	0.038–0.780	1.1–8.4	8	0.9961
Hermes12(p)	[51]	0.039–0.678	1.09–10.35	20	0.9992
SMC(p)	[52]	0.010–0.378	1.36–17.07	6	1.0000
g_2^p				**46**	
E143(d)	[35]	0.038–0.595	1.49–8.86	12	1.0001
E155(d)	[50]	0.038–0.780	1.1–8.2	8	1.0005
g_2^d				**20**	
E143(n)	[35]	0.038–0.595	1.49–8.86	12	1.0000
E155(n)	[50]	0.038–0.780	1.1–8.8	8	0.9995
E142(n)	[45]	0.036–0.466	1.1–5.5	8	1.0000
Jlab03(n)	[49]	0.14–0.22	1.09–1.46	4	0.9928
Jlab04(n)	[48]	0.33–0.60	2.71–4.83	3	0.9477
Jlab05(n)	[2]	0.19–0.20	1.13–1.34	2	0.9888
g_2^n				**37**	
Total				**517**	

C. Method of minimization and error calculation

$\chi^2(p)$ quantifies the goodness of fit to the data for a set of independent parameters p that specifies the PDFs at Q_0^2 [53]:

$$\chi^2_{\text{global}}(p) = \sum_{i=1}^{n^{\text{exp}}} \left[\left(\frac{\mathcal{N}_i - 1}{\Delta \mathcal{N}_i} \right)^2 + \sum_{j=1}^{n^{\text{data}}} \left(\frac{\mathcal{N}_i g_j^{\text{data}} - g_j^{\text{theory}}(p)}{\mathcal{N}_i \Delta g_j^{\text{data}}} \right)^2 \right]. \quad (14)$$

n^{exp} and n^{data} are the number of individual experimental data sets and corresponding number of data points included in each data set, respectively. For the ith experiment, each data value g_j^{data} with measurement uncertainty Δg_j^{data} is compared to the corresponding theoretical value g_j^{theor}. The correlated normalization uncertainty $\Delta \mathcal{N}_i$ is reported for most experiments. $\Delta \mathcal{N}_i$ is the experimental normalization uncertainty, and $\mathcal{N}_i$ is an overall normalization factor for the data of experiment i. We allow for a relative normalization shift $\mathcal{N}_i$ between different data sets within uncertainties $\Delta \mathcal{N}_i$ quoted by the experiments. The minimization of the above χ^2 function is done using the program MINUIT [54].

IV. DISCUSSION OF FIT RESULTS

In this section, we describe our fit, which was performed including target mass corrections to the leading twist contributions and considering higher twist terms. We extract the pure twist-2 and twist-3 contributions along with strong coupling constant.

The standard scenario to extract PDFs from observable is to consider a certain functional form in the leading twist in the $\overline{\text{MS}}$ scheme as our reference distribution. Their scale dependence is given by the well-known DGLAP evolution equations. Here, we have performed all Q^2 evolutions in Mellin space using the QCD-PEGASUS program [55] in the fixed flavor number scheme. The number of active flavors in the splitting functions and Wilson coefficients is fixed at $N_f = 3$.

A. Polarized PDFs

In our QCD analysis, we perform two fitting scenarios to distinguish the effect of target mass corrections and higher twist contribution. These contributions are both considered in the "full scenario," while the "pQCD scenario" is based on the twist-2 NLO pQCD g_1 and twist-2 WW g_2 (see Table I). In the following sections, we indicate full scenario by "model."

The χ^2 fit value of the full scenario is smaller than the pQCD scenario, indicating the importance of low-Q^2 corrections. It supports our theoretical framework in which the leading twist part is enriched by TMCs and HT terms.

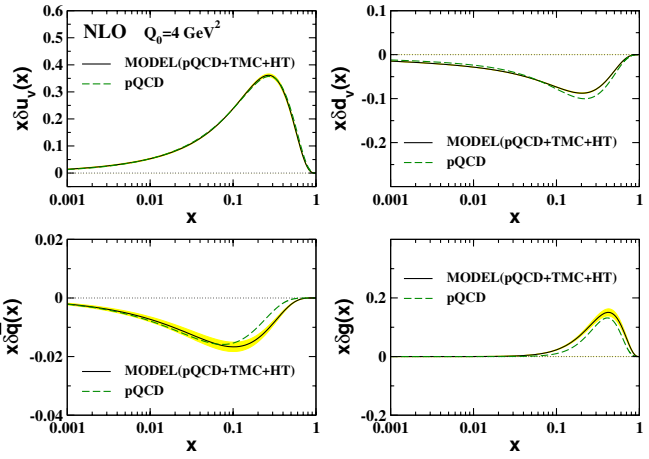

FIG. 1 (color online). The polarized parton distribution at $Q_0^2 = 4$ GeV^2 as a function of x. Our model is represented by the solid curve, and the pQCD scenario is representend by the dashed curve.

As shown in Table I, the precision of the extracted PPDFs is essentially enhanced, which is a consequence of above discussed corrections. The strong coupling constant receives corrections of 0.003 at a scale of Q_0^2.

We compare the PPDFs extracted based on these two scenarios in Fig. 1. Large-x sea distribution is the most affected part, while $x\delta u_V$ is the least. In Fig. 2, we compared our model with various parametrizations from the literature [10–12,14,17,56]. Most of the fits are comparable. The differences originate from the choice of data sets, the form of PPDF parametrization, and several details of the QCD analysis. For example, the LSS analysis [17] considered the impact of higher twist corrections on their PPDFs, or the DSSV study [10] included semi-inclusive

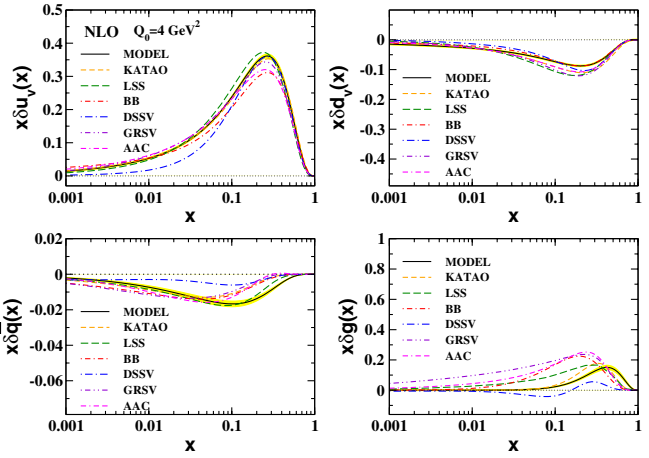

FIG. 2 (color online). The polarized parton distribution at $Q_0^2 = 4$ GeV^2 as a function of x. Our fit is the solid curve. Also shown are the results of KATAO (dashed) [14], LSS (long dashed) [17], BB (dashed dotted) [11], DSSV (long dashed dotted) [10], GRSV (dashed-dotted dotted) [56], and AAC (long dashed-dashed dotted) [12].

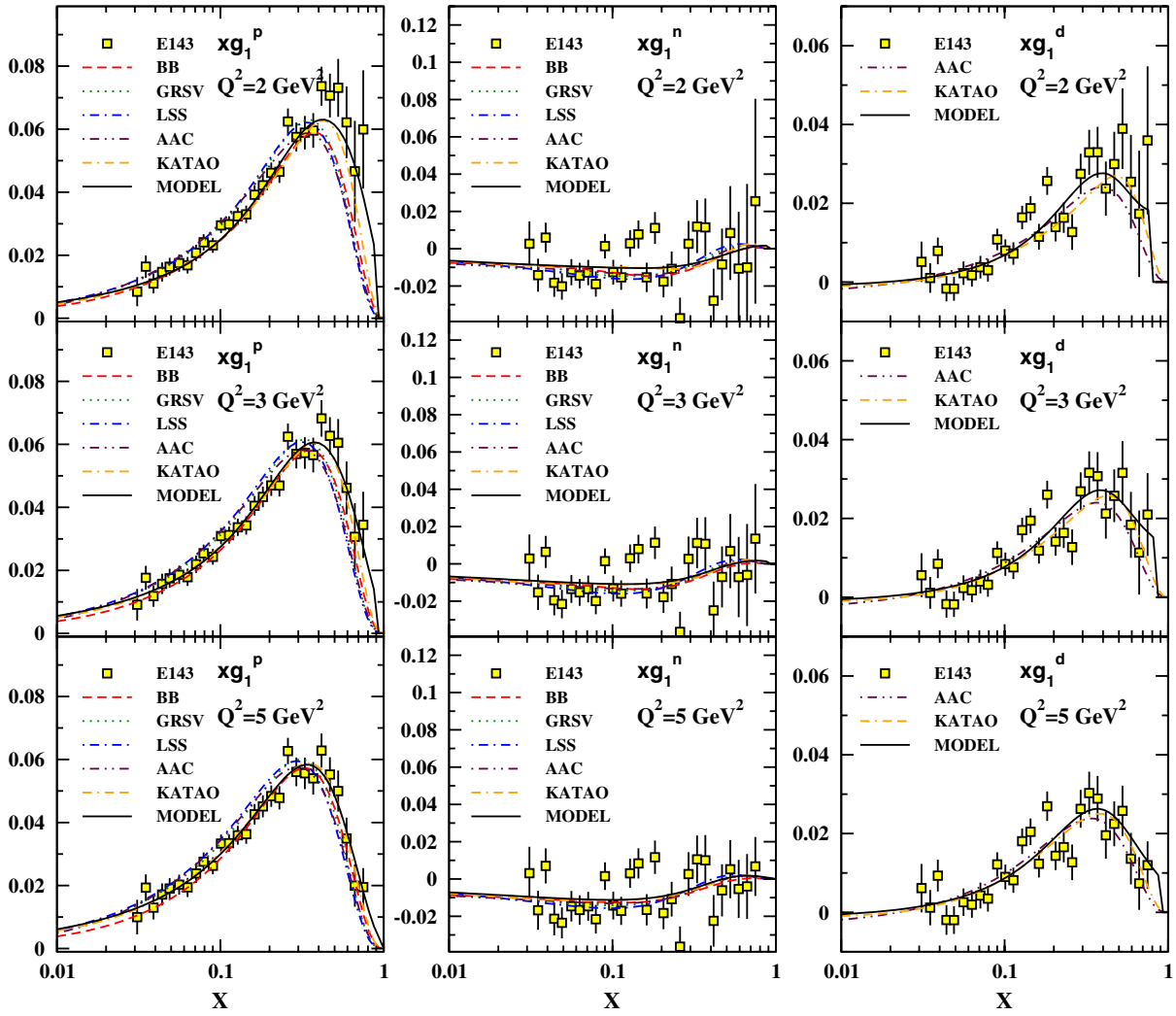

FIG. 3 (color online). The polarized structure functions as a function of x and for different low values of Q^2. Our result (solid curve) is compared with the curves obtained by BB (dashed) [57], GRSV (dotted) [56], LSS (dashed dotted) [58], AAC (dashed-dotted dotted) [59], and KATAO (dashed-dashed dotted) [14].

data in its fitting pass and had different curves for $\bar{u}$, $\bar{d}$, and $\bar{s}$.

B. Polarized structure functions

In Fig. 3, we plot our results for $xg_1^{p,n,d}(x, Q^2)$ as a function of x for low values of Q^2. The effect of the θ function is visible in large x. Our curves are well described by the data. Figure 4 shows our prediction for $g_1^p(x, Q^2)$ as a function of Q^2 and for different values of x, in comparison with the others [14,56–60]. The data are well described within errors. Despite the limited range in Q^2, scaling violations of g_1 are obviously visible. The xg_2 polarized structure functions for the proton, neutron, and deuteron are shown as a function of x in Fig. 5. We compare our results based on two scenarios with the experimental data from Refs. [2,35,48–52]. In Fig. 6, xg_2^p as a function of Q^2 is compared with experimental data [35,50–52].

C. HT contributions

Our results for the twist-3 contribution of both polarized structure functions are shown at $Q^2 = 1, 3, 5, 10$ in Figs. 7 and 8. Note that they vanish with the evolution in the high-Q^2 regime. A significant positive twist-3 modification observes for $g_{2,p}^{tw-3}$ at $x \geq 0.3$, which is even larger than the $g_{1,p}^{tw-3}$ modification and as shown in Fig. 5, cancels some of the negative leading twist contribution. On the contrary, the $g_{2,n}^{tw-3}$ is approximately zero. A similar result is reported in Ref. [8].

In Fig. 9, we compare our result on twist-3 contributions to g_1^p with those obtained by LSS [17] and JAM [8]. The LSS group extracted effective HT in a model-independent way from experimental data corresponding to seven x bins. However, the logarithmic Q^2 dependence of the twist-3 parts is neglected. The JAM global NLO analysis is based on a direct fit of the measured longitudinal and transverse

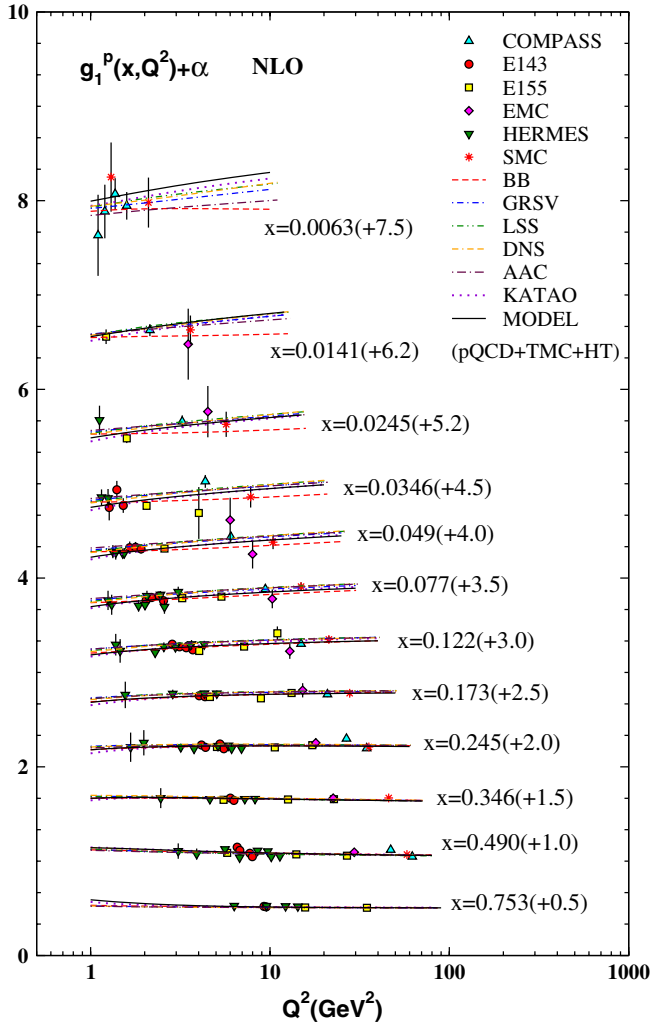

FIG. 4 (color online). The structure function $g_1^p(x, Q^2)$ as a function of Q^2 in different intervals of x compared to experimental data. Also shown are the results of BB (dashed) [57], GRSV (dashed dotted) [56], LSS (dashed-dotted dotted) [58], DNS (dashed-dashed dotted) [60], AAC (long dashed dotted) [59], and KATAO (dotted) [14]. To improve legibility, the values of $g_1(x, Q^2)$ have been shifted by the amount of α.

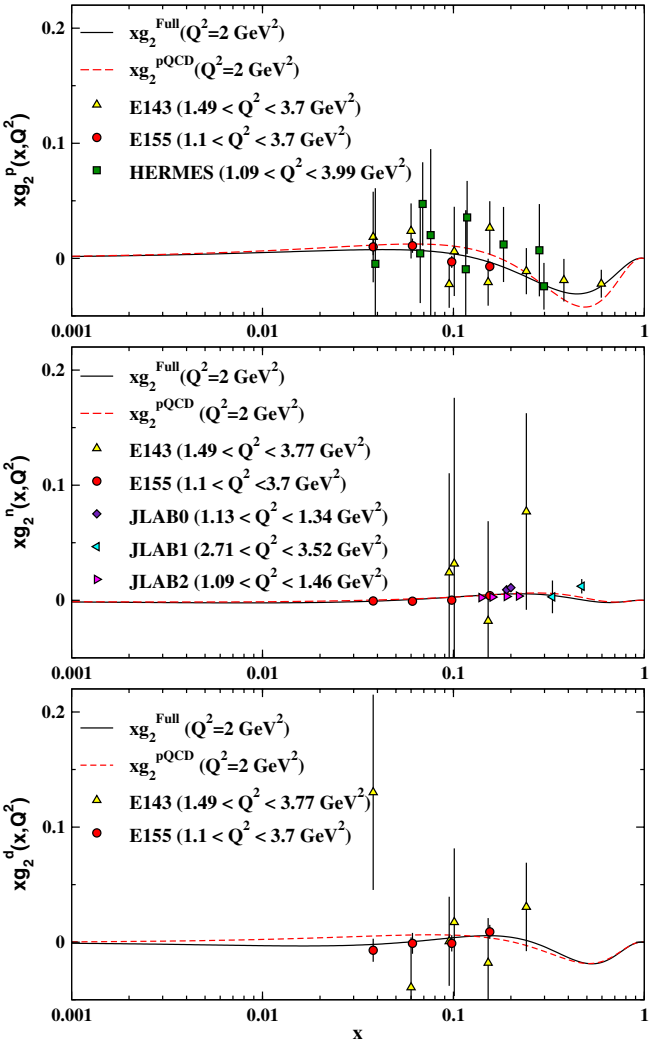

FIG. 5 (color online). The structure function xg_2 at $Q^2 = 2$ GeV^2 as a function of x compared to experimental data.

asymmetries. In Fig. 10, the twist-3 contribution to xg_2 is compared with the JAM [8] and BLMP models [33] along with the E143 experimental data [35]. Our results are comparable with theoretical and phenomenological predictions.

D. Strong coupling constant

In our analysis, the strong coupling constant is considered as a free parameter. Although some phenomenological groups, such as LSS [9,17] or AKS [15], fix α_s close to the updated Particle Data Group average, other phenomenological groups, such as BB [11,57] or KATAO [14], extract it as a free parameter. To take into account its correlation with other parameters, the strong coupling constant extracted simultaneously with the PPDFs and higher twist terms. We achieve the value of $\alpha_s(Q_0^2) = 0.365 \pm 0.011$ in our model. This value is closely related to the gluon distribution, which drives the QCD evolution.

The scale dependence of the running coupling constant at NLO is precisely given in terms of $a_s(Q_0^2)$ by

$$\frac{1}{a_s(Q^2)} = \frac{1}{a_s(Q_0^2)} + \beta_0 \ln\left(\frac{Q^2}{Q_0^2}\right) - b_1 \ln\left\{\frac{a_s(Q^2)[1 + b_1 a_s(Q_0^2)]}{a_s(Q_0^2)[1 + b_1 a_s(Q^2)]}\right\}. \quad (15)$$

Here, $a_s = \frac{\alpha_s}{4\pi}$ and $b_1 = \frac{\beta_1}{\beta_0}$. The β functions are known up to next-to-next-to-next-to-leading order and depend on the number of active flavors [61–64]. Rescaling the coupling constant to the Z boson mass, we obtain $\alpha_s(M_Z^2) = 0.1136 \pm 0.0012$, which is comparable with the current world average $\alpha_s(M_Z^2) = 0.1184 \pm 0.0007$.

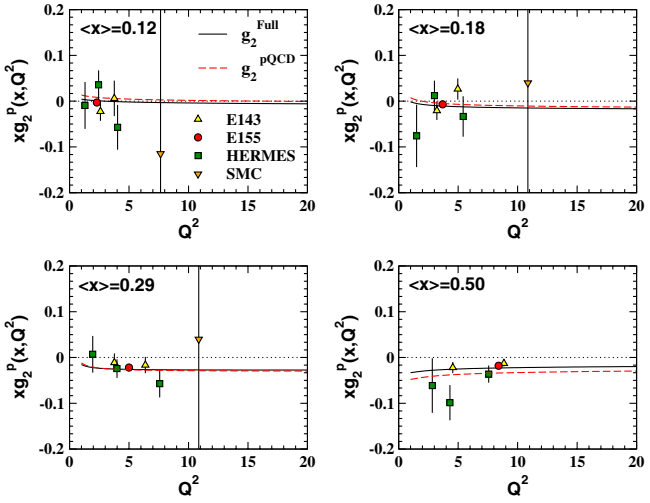

FIG. 6 (color online). The polarized structure function xg_2^p as a function of Q^2 and for different values of x compared with experimental data.

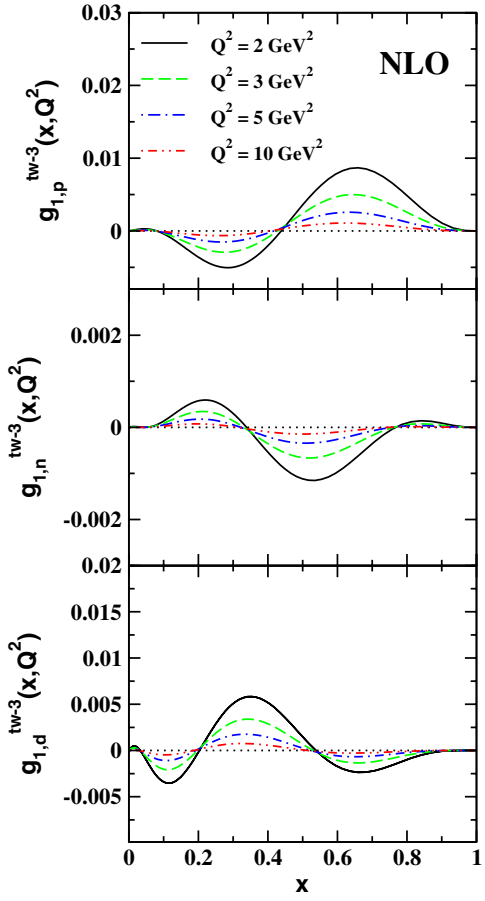

FIG. 7 (color online). The twist-3 contribution of g_1 for the proton, neutron, and deuteron as a function of x and for different values of Q^2.

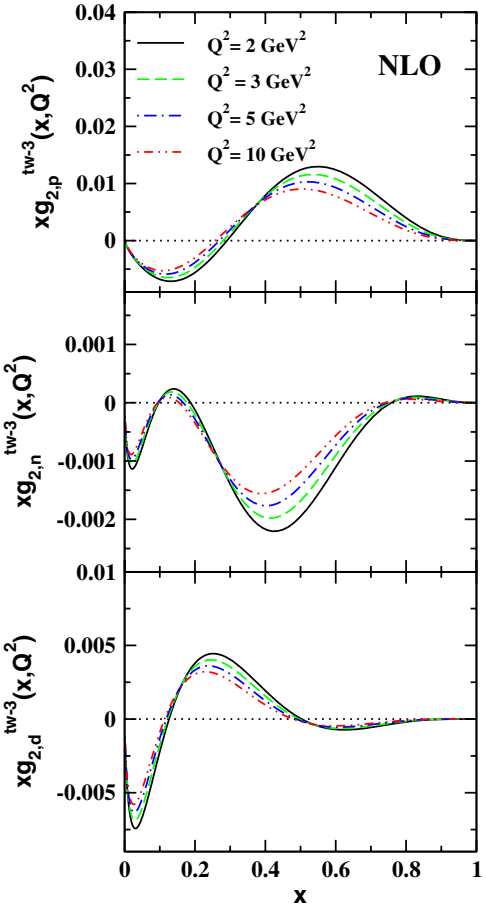

FIG. 8 (color online). The twist-3 contribution of xg_2 for the proton, neutron, and deuteron as a function of x and for different values of Q^2.

V. POLARIZED STRUCTURE FUNCTION OF ^{3}He AND ^{3}H

^{3}He and ^{3}H are two of simplest nuclei, which consist of 2(1) protons and 1(2) neutron. Because of different nuclear effects, protons and neutrons inside the nuclei are different from those in free space. The most important effects are spin depolarization, nuclear binding, and Fermi motion, which are available in the framework of the convolution approach [65]. In this approximation, $g_1^{^3\mathrm{He}}$ and $g_1^{^3\mathrm{H}}$ can be interpreted as the convolution of g_1^p and g_1^n with the spin-dependent nucleon light-cone momentum distributions $\Delta f^N_{(^3\mathrm{He},^3\mathrm{H})}(y)$ as follows [66,67]:

$$g_1^{^3\mathrm{He}}(x,Q^2) = \int_x^3 \frac{dy}{y}\Delta f^n_{^3\mathrm{He}}(y) g_1^n\left(\frac{x}{y},Q^2\right) + 2\int_x^3 \frac{dy}{y}\Delta f^p_{^3\mathrm{He}}(y) g_1^p\left(\frac{x}{y},Q^2\right) - 0.014[g_1^p(x,Q^2) - 4g_1^n(x,Q^2)], \quad (16)$$

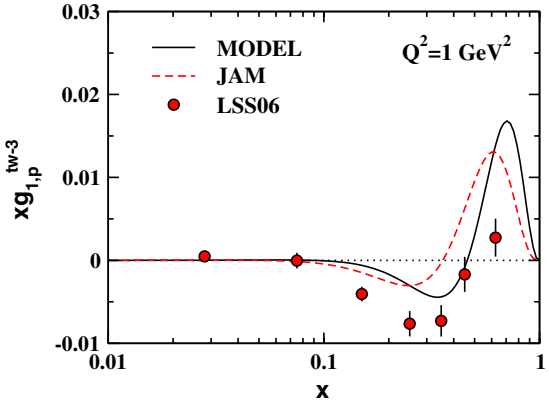

FIG. 9 (color online). The twist-3 contribution to xg_1 at $Q^2 = 1$ GeV^2 as a function of x compared to the results of LSS [17] and JAM [8].

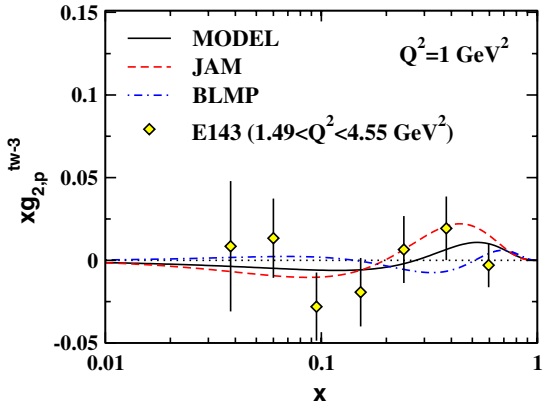

FIG. 10 (color online). The twist-3 contribution to xg_2 at $Q^2 = 1$ GeV^2 as a function of x. The current fit is the solid curve. Also shown are the curve based on JAM [8] (dashed), BLMP [33] (dashed dotted), and E143 experimental data.

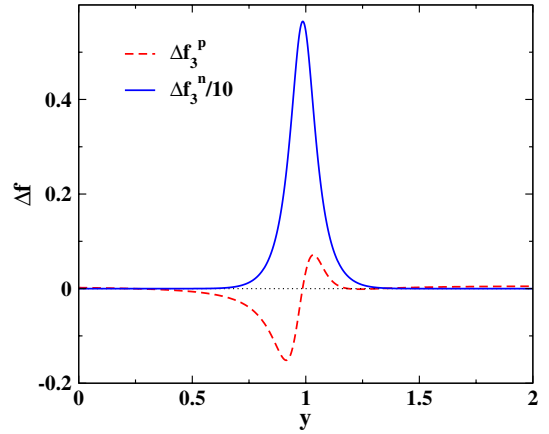

FIG. 11 (color online). The polarized light-cone distribution functions for proton and neutron in ^{3}He.

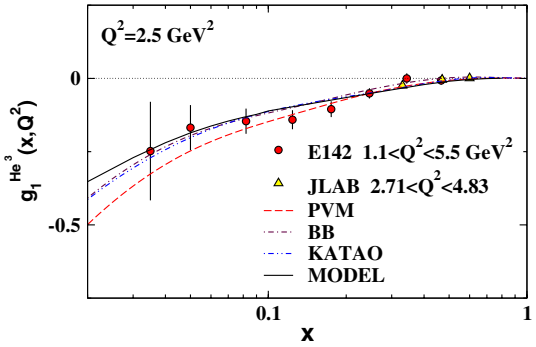

FIG. 12 (color online). $g_1^{\mathrm{He}^3}$ for fixed $Q^2 = 2.5$ GeV^2. The current fit is the solid curve. Also shown are the curves based on the polarized valon model (PVM) (dashed) [70], BB (dashed dotted) [57], and KATAO (dashed-dotted dotted) [14].

$$g_1^{^3\mathrm{H}}(x,Q^2) = 2\int_x^3 \frac{dy}{y}\Delta f^n_{^3\mathrm{H}}(y) g_1^n\left(\frac{x}{y},Q^2\right) + \int_x^3 \frac{dy}{y}\Delta f^p_{^3\mathrm{H}}(y) g_1^p\left(\frac{x}{y},Q^2\right) + 0.014[g_1^p(x,Q^2) - 4g_1^n(x,Q^2)]. \quad (17)$$

$\Delta f^N_{(^3\mathrm{He},^3\mathrm{H})}(y)$ is the probability to find N in the $(^3\mathrm{He},^3\mathrm{H})$ with a given fraction of the total momentum y. The light-cone momentum distributions for the proton and neutron in the three-nucleon system is determined. Concerning isospin symmetry, $f^p_{^3\mathrm{He}}(f^n_{^3\mathrm{He}})$ and $f^n_{^3\mathrm{H}}(f^p_{^3\mathrm{H}})$ are equal.

We used the results of Refs. [65,68,69] as

$$\Delta f^n_{^3\mathrm{He}}(y) = \frac{a^n e^{-\frac{0.5(1-d^n)(-b^n+y)^2}{(c^n)^2}}}{1+\frac{d^n(-b^n+y)^2}{(c^n)^2}}, \quad (18)$$

$$\Delta f^p_{^3\mathrm{He}}(y) = \frac{\sum_{i=0}^4 a_i^p U_i(y)}{\sum_{i=0}^4 b_i^p U_i(y)}. \quad (19)$$

Here, $U_n(y)$ is the Chebyshev polynomial of the second kind. The numerical multipliers of the above equations are

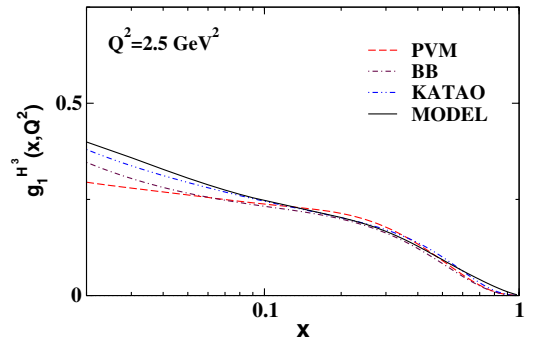

FIG. 13 (color online). $g_1^{\mathrm{H}^3}$ for fixed $Q^2 = 2.5$ GeV^2. The current fit is the solid curve. Also shown are the curves based on the polarized valon model (PVM) (dashed) [70], BB (dashed dotted) [57], and KATAO (dashed-dotted dotted) [14].

discussed in Ref. [14]. Figure 11 represents our polarized light-cone distribution, which is written based on numerical results of Ref. [69].

Our results for $g_1^{^3\mathrm{He}}$ and $g_1^{^3\mathrm{H}}$ are compared with BB [57], PVM [70], and KATAO [14] in Figs. 12 and 13.

VI. SUM RULES

Parton distribution functions and structure functions follow a series of sum rules. These sum rules, which are based on the moments of structure functions, provide an opportunity to test QCD. Moments of structure functions contain valuable information about the total momentum fraction carried by partons or the total contribution of parton helicities to the spin of nucleon in unpolarized or polarized cases. Ellis–Jaffe [71] and Bjorken [72] sum rules are based on the first moment of g_1. The Burkhard–Cottingham [73] sum rule focuses on the first moment of g_2. Moreover, moments of $g_{1,2}$ can be related to matrix elements operators via the OPE. All these important sum rules are briefly discussed in following.

A. Twist-3 contributions to polarized nucleon structure functions sum rule

The OPE sum rule relates the moments of g_1 and g_2 at fixed Q^2 to the twist-2 and twist-3 reduced matrix elements of spin-dependent operators in the nucleon, a_n and d_n [74],

$$\Gamma_1^n = \int_0^1 x^n g_1(x,Q^2)dx = \frac{a_n}{2}, \quad n = 0,2,4,\ldots$$
$$\Gamma_2^n = \int_0^1 x^n g_2(x,Q^2)dx = \frac{1}{2}\frac{n}{n+1}(d_n - a_n), \quad n = 2,4,\ldots \tag{20}$$

For the first moment of g_2 ($\int_0^1 g_2(x,Q^2)dx$), the OPE does not define any sum rule. But Burkhardt and Cottingham have derived this value from virtual Compton scattering dispersion relations, which will be discussed in the next part.

The twist-3 matrix elements,

$$d_n(Q^2) = 2\int_0^1 x^n \left(\frac{n+1}{n}\right)\bar{g}_2(x,Q^2)dx, \qquad n = 2,4,6,\ldots, \tag{21}$$

measure deviations of g_2 from g_2^{ww} term [see Eq. (4)].

Having a number of theoretical [75–80] and experimental [35,81] nonzero predictions for d_2, which indicate on the role of twist-3 contribution, makes the study of g_2 specifically exciting. In Tables IV and V, we quote theoretical and experimental values for the twist-2 and twist-3 matrix elements for the proton, neutron, and deuteron together with our results. This remarkably nonzero value for d_2 indicates the importance of considering higher twist approximation. The accuracy of the current data is not sufficient enough to specify model precision.

B. Burkhardt–Cottingham sum rule

The first moment of $g_2(x,Q^2)$ follows the Burkhardt–Cottingham (BC) sum rule for all Q^2 [73]:

$$\int_0^1 dx[g_2(x,Q^2)] = 0. \tag{22}$$

Its validity depends on the lack of singularities for g_2 at $x \to 0$. Note that this sum rule would automatically be satisfied in twist 2. Therefore, the presence of higher twist contributions can be concluded from the sum rule violation [51]. In Table VI, our result for this sum rule at $Q^2 = 5$ GeV^2 is compared with experimental results [35,50,51]. Any conclusion relies on the behavior of g_2 at low x, which is not accurately known up to now.

C. Bjorken sum rule

The Bjorken sum rule [72] relates the integral over all x at fixed Q^2 of the difference between the proton and neutron polarized structure function to the neutron beta decay coupling constant. This sum rule can be explicitly concluded for the ^{3}He–^{3}H system. Considering the ratio of these two relations, one gets [65]

$$\frac{\int_0^3 [g_1^{^3\mathrm{H}}(x,Q^2) - g_1^{^3\mathrm{He}}(x,Q^2)]dx}{\int_0^1 [g_1^p(x,Q^2) - g_1^n(x,Q^2)]dx} = \frac{\tilde{g}_A}{g_A} = 0.956 \pm 0.004. \tag{23}$$

We achieved the value of 0.974 for the above ratio.

D. Ellis–Jaffe sum rule

The first moment of g_1 for the proton and neutron was calculated by Ellis–Jaffe sum rules,

TABLE IV. Comparison of theoretical and experimental results for the reduced twist-2 matrix element proton, neutron, and deuteron.

	Ref.	Q^2 [GeV^2]	a_2^p	a_2^n	a_2^d
Model		5	2.22×10^{-2}	-3.6×10^{-4}	9.97×10^{-3}
Center of mass bag model	[75]	5	2.10×10^{-2}	-1.86×10^{-3}	8.74×10^{-3}
Lattice QCD	[76]	4	$(3.00 \pm 0.64) \times 10^{-2}$	$-(2.4 \pm 4.0) \times 10^{-3}$	$(13.8 \pm 5.2) \times 10^{-3}$
E143	[35]	5	$(2.48 \pm 0.20) \times 10^{-2}$	$-(4.8 \pm 3.2) \times 10^{-3}$	$(9.2 \pm 1.6) \times 10^{-3}$

TABLE V. Comparison of theoretical and experimental results for the reduced twist-3 matrix element proton, neutron, and deuteron.

	Ref.	Q^2 [GeV^2]	d_2^p	d_2^n	d_2^d
Model		5	0.58×10^{-2}	-0.7×10^{-3}	0.6×10^{-3}
JAM model	[8]	5	1.1×10^{-2}	2×10^{-3}	–
Center of mass bag model	[75]	5	1.74×10^{-2}	-2.53×10^{-3}	6.79×10^{-3}
MIT bag model	[77,78]	1	1.0×10^{-2}	0	5.0×10^{-3}
QCD sum rule	[79]	1	$-(0.6 \pm 0.3) \times 10^{-2}$	$-(30 \pm 10) \times 10^{-3}$	$-(17 \pm 5) \times 10^{-3}$
QCD sum rule	[80]	1	$-(0.3 \pm 0.3) \times 10^{-2}$	$-(25 \pm 10) \times 10^{-3}$	$-(13 \pm 5) \times 10^{-3}$
Lattice QCD	[76]	4	$-(4.8 \pm 0.5) \times 10^{-2}$	$-(3.9 \pm 2.7) \times 10^{-3}$	$-(22 \pm 6) \times 10^{-3}$
Combined E155 with SLAC data	[81]	5	$(0.32 \pm 0.17) \times 10^{-2}$	$(0.79 \pm 0.48) \times 10^{-2}$	–
E143	[35]	5	$(0.58 \pm 0.50) \times 10^{-2}$	$(5.0 \pm 21.0) \times 10^{-3}$	$(5.1 \pm 9.2) \times 10^{-3}$

TABLE VI. Comparison of the result of the Burkhardt–Cottingham sum rule with experimental data in $Q^2 = 5$ GeV^2. Our result is calculated in two different x ranges.

	E143 [35] $0.03 \le x \le 1$	E155 [50] $0.02 \le x \le 0.8$	HERMES2012 [51] $0.023 \le x \le 0.9$	Model $0(0.02) \le x \le 1(0.9)$
$\int g_2^p(x, Q^2)dx$	-0.014 ± 0.028	$-0.044 \pm 0.008 \pm 0.003$	$0.006 \pm 0.024 \pm 0.017$	$-0.008(-0.012)$
$\int g_2^d(x, Q^2)dx$	-0.034 ± 0.082	$-0.008 \pm 0.012 \pm 0.002$	–	$-0.003(-0.006)$

TABLE VII. Comparison of the result of Ellis–Jaffe sum rule with experimental data in $Q^2 = 5$ GeV^2. Hermes [40] results are measured in the region $0.021 \le x \le 0.9$.

	E143 [35]	SMC [52]	HERMES [40]	Model
$\int g_1^p(x, Q^2)dx$	$0.129 \pm 0.003 \pm 0.010$	0.132 ± 0.017	0.121 ± 0.009	0.121 ± 0.002
$\int g_1^n(x, Q^2)dx$	$-0.034 \pm 0.007 \pm 0.016$	-0.048 ± 0.022	-0.027 ± 0.009	-0.027 ± 0.004
$\int g_1^d(x, Q^2)dx$	$0.044 \pm 0.003 \pm 0.006$	0.039 ± 0.008	0.044 ± 0.003	0.034 ± 0.003

$$\int_0^1 g_1^p(x, Q^2)dx = \frac{g_A}{12}(1.78),$$
$$\int_0^1 g_1^n(x, Q^2)dx = \frac{g_A}{12}(-0.22), \quad (24)$$

where $g_A = 1.248 \pm 0.010$ [71]. The α_s^3 corrections to these sum rules were calculated in Ref. [82]. The Ellis–Jaffe sum rules are not as fundamental as the Bjorken sum rule since they are derived based on a model-dependent assumption that strange quarks do not contribute to the asymmetry. However, they teach us about the spin structure of the nucleon. Our result for this sum rule, in the x range of $0.021 \le x \le 0.9$, is compared with experimental measurements [35,40,52] in Table VII.

E. Efremov–Leader–Teryaev sum rule

This sum rule involves only the valence contributions of the polarized structure functions $g_{1,2}$ [83]:

$$\int_0^1 dx x[g_1^V(x) + 2g_2^V(x)] = 0. \quad (25)$$

Assuming the isospin symmetry of the sea quark distribution, the sum rule takes a form $\int_0^1 dx x[g_1^p(x) + 2g_2^p(x) - g_1^n(x) - 2g_2^n(x)] = 0$. It holds under the presence of target mass corrections [25]. We achieved the amount of 1.78×10^{-5} at $Q^2 = 5$ GeV^2, which is consistent with zero. The value of $-0.013 \pm 0.008 \pm 0.002$ is reported by E155 [50] at the same Q^2.

F. First moment

The spin contribution of parton i to the nucleon spin can be found by its first moment integral $\Delta q_i(Q^2) = \int_0^1 dx \delta q_i(x, Q^2)$. This is why there are universal efforts to determine the $\delta q_i(x, Q^2)$ from different experimental data. In Table VIII, we present the values for the first moments of the polarized quark and gluon extracted from our model at $Q_0^2 = 4$ GeV^2. They are compared with recent fit results of DSSV08 [10] [DIS, semi-inclusive deep inelastic scattering (SIDIS), and RHIC], BB10 [11] (DIS data), LSS10 [9] (DIS and SIDIS data), AAC08-Set A [12] (DIS), and NFRR12 [84] (DIS data). The values of $\Delta\Sigma$ are almost comparable, while different Δg are reported.

TABLE VIII. First moments of the polarized singlet-quark $\Delta\Sigma(Q^2) = \sum_i \int_0^1 dx[\delta q_i(x) + \delta\bar{q}_i(x)]$ and gluon distributions at the scale $Q_0^2 = 4$ GeV^2 in the $\overline{\text{MS}}$ -scheme (only AAC08 [12] results are given at $Q_0^2 = 1$ GeV^2).

	DSSV08 [10]	BB10 [11]	LSS10 [9]	AAC08[12]	NFRR12 [84]	Model
$\Delta\Sigma(Q^2)$	0.25 ± 0.02	0.19 ± 0.08	0.21 ± 0.03	0.24 ± 0.07	0.31 ± 0.10	0.223 ± 0.036
$\Delta g(Q^2)$	-0.10 ± 0.16	0.46 ± 0.43	0.32 ± 0.19	0.63 ± 0.81	-0.2 ± 1.4	0.201 ± 0.044

VII. CONCLUSIONS

We have carried out a NLO QCD analysis to the polarized structure functions data g_1 and g_2. During the analysis, we considered TMCs and HT effects to extract the PPDFs inside the nucleon. The strong coupling constant and twist-3 part of the g_1 and g_2 are simultaneously determined along with them. The TMCs are calculated explicitly from the leading twist perturbative polarized structure function within the OPE. In contrast to most previous PPDFs studies that neglected the scale dependence of the HT contributions, our model considers the Q^2 evolution of the HT terms. This strategy leads to extracting more precise PPDFs with smaller uncertainty bands. We report smaller χ^2 for our full scenario including low Q^2 corrections. This progress demonstrates a clear preference of the data for the existence of their effects. The strong coupling constant also receives a small correction. Having extracted the polarized PDFs, we estimated the nuclear structure function of ^{3}He and ^{3}H. Finally, we computed the moments of PPDFs and structure functions and discussed the sum rules. We found good agreement with the observables, and our outcomes were agreeable with other results from the literature. More accurate data are required to conclude final determination.

Having analyzed all the polarized inclusive DIS data on g_1 and g_2, we examined the efficiency of our method on SIDIS data to calculate quark and antiquark densities individually. This work is in progress.

ACKNOWLEDGMENTS

The authors appreciate E. Leader for reading the manuscript of this paper, fruitful suggestions, and critical remarks. S. T. thanks the CERN TH-PH division for its hospitality where a portion of this work was performed. A. N. K. is grateful to the Physics Department of Southern Methodist University for its hospitality. S. T. and A. N. K. acknowledge the School of Particles and Accelerators, Institute for Research in Fundamental Sciences (IPM), for financially supporting this project.

APPENDIX: FORTRAN CODE

A FORTRAN package containing our PPDFs as well as the polarized structure functions $g_{1,2}(x, Q^2)$ together with the g_2^{tw-3} contribution for the proton, neutron, and deuteron is available in http://particles.ipm.ir/links/QCD.htm or can be obtained via Email from the authors. These functions are interpolated using cubic splines in Q^2 and a linear interpolation in $\log(Q^2)$. The package includes an example program to illustrate the use of the routines.

[1] K. Abe *et al.* (E154 Collaboration), Phys. Lett. B **404**, 377 (1997).
[2] K. Kramer *et al.*, Phys. Rev. Lett. **95**, 142002 (2005).
[3] A. D. Martin, W. J. Stirling, R. S. Thorne, and G. Watt, Eur. Phys. J. C **63**, 189 (2009).
[4] J. Gao, M. Guzzi, J. Huston, H.-L. Lai, Z. Li, P. Nadolsky, J. Pumplin, D. Stump, and C.-P. Yuan, Phys. Rev. D **89**, 033009 (2014).
[5] I. Schienbein *et al.*, J. Phys. G **35**, 053101 (2008).
[6] S. Simula, M. Osipenko, G. Ricco, and M. Taiuti, Phys. Rev. D **65**, 034017 (2002).
[7] R. D. Ball, V. Bertone, S. Carrazza, L. D. Debbio, S. Forte, A. Guffanti, N. P. Hartland, and J. Rojo (NNPDF Collaboration), Nucl. Phys. **B877**, 290 (2013).
[8] P. Jimenez-Delgado, A. Accardi, and W. Melnitchouk, Phys. Rev. D **89**, 034025 (2014).
[9] E. Leader, A. V. Sidorov, and D. B. Stamenov, Phys. Rev. D **82**, 114018 (2010).
[10] D. de Florian, R. Sassot, M. Stratmann, and W. Vogelsang, Phys. Rev. Lett. **101**, 072001 (2008); D. de Florian, R. Sassot, M. Stratmann, and W. Vogelsang, Phys. Rev. D **80**, 034030 (2009).
[11] J. Blumlein and H. Bottcher, Nucl. Phys. **B841**, 205 (2010).
[12] M. Hirai and S. Kumano (Asymmetry Analysis Collaboration), Nucl. Phys. **B813**, 106 (2009).
[13] C. Bourrely, J. Soffer, and F. Buccella, Eur. Phys. J. C **23**, 487 (2002).
[14] A. N. Khorramian, S. Atashbar Tehrani, S. Taheri Monfared, F. Arbabifar, and F. I. Olness, Phys. Rev. D **83**, 054017 (2011).
[15] F. Arbabifar, A. N. Khorramian, and M. Soleymaninia, Phys. Rev. D **89**, 034006 (2014).
[16] E. Leader, A. V. Sidorov, and D. B. Stamenov, Phys. Rev. D **80**, 054026 (2009).
[17] E. Leader, A. V. Sidorov, and D. B. Stamenov, Phys. Rev. D **75**, 074027 (2007).

[18] E. Leader, A. V. Sidorov, and D. B. Stamenov, Phys. Rev. D **67**, 074017 (2003).
[19] D. Boer *et al.*, arXiv:1108.1713.
[20] M. Anselmino, A. Efremov, and E. Leader, Phys. Rep. **261**, 1 (1995) **281**, 399(E) (1997)].
[21] B. Lampe and E. Reya, Phys. Rep. **332**, 1 (2000).
[22] S. Wandzura and F. Wilczek, Phys. Lett. B **72**, 195 (1977).
[23] A. Piccione and G. Ridolfi, Nucl. Phys. **B513**, 301 (1998).
[24] A. Accardi, A. Bacchetta, W. Melnitchouk, and M. Schlegel, J. High Energy Phys. 11 (2009) 093.
[25] J. Blumlein and A. Tkabladze, Nucl. Phys. **B553**, 427 (1999).
[26] O. Nachtmann, Nucl. Phys. **B63**, 237 (1973).
[27] Y. B. Dong, Phys. Lett. B **641**, 272 (2006).
[28] A. Accardi and W. Melnitchouk, Phys. Lett. B **670**, 114 (2008).
[29] H. Georgi and H. D. Politzer, Phys. Rev. D **14**, 1829 (1976).
[30] A. De Rujula, H. Georgi, and H. D. Politzer, Phys. Rev. D **15**, 2495 (1977).
[31] R. K. Ellis, W. Furmanski, and R. Petronzio, Nucl. Phys. **B221**, 29 (1983).
[32] U. D'Alesio, E. Leader, and F. Murgia, Phys. Rev. D **81**, 036010 (2010).
[33] V. M. Braun, T. Lautenschlager, A. N. Manashov, and B. Pirnay, Phys. Rev. D **83**, 094023 (2011).
[34] C. Amsler *et al.*. (Particle Data Group), Phys. Lett. B **667**, 1 (2008).
[35] K. Abe *et al.* (E143 collaboration), Phys. Rev. D **58**, 112003 (1998).
[36] A. Airapetian *et al.* (HERMES Collaboration), Phys. Lett. B **442**, 484 (1998).
[37] B. Adeva *et al.* (Spin Muon Collaboration), Phys. Rev. D **58**, 112001 (1998).
[38] J. Ashman *et al.* (European Muon Collaboration), Phys. Lett. B **206**, 364 (1988); J. Ashman *et al.* (European Muon Collaboration), Nucl. Phys. **B328**, 1 (1989).
[39] P. L. Anthony *et al.* (E155 Collaboration), Phys. Lett. B **493**, 19 (2000).
[40] A. Airapetian *et al.* (HERMES Collaboration), Phys. Rev. D **75**, 012007 (2007).
[41] M. G. Alekseev *et al.* (COMPASS Collaboration), Phys. Lett. B **690**, 466 (2010); V. Y. Alexakhin *et al.* (COMPASS Collaboration), Phys. Lett. B **647**, 8 (2007).
[42] P. L. Anthony *et al.* (E155 Collaboration), Phys. Lett. B **463**, 339 (1999).
[43] E. S. Ageev *et al.* (COMPASS Collaboration), Phys. Lett. B **612**, 154 (2005).
[44] V. Y. Alexakhin *et al.* (COMPASS Collaboration), Phys. Lett. B **647**, 8 (2007).
[45] P. L. Anthony *et al.* (E142 Collaboration), Phys. Rev. D **54**, 6620 (1996).
[46] K. Abe *et al.* (E154 Collaboration), Phys. Rev. Lett. **79**, 26 (1997).
[47] K. Ackerstaff *et al.* (HERMES Collaboration), Phys. Lett. B **404**, 383 (1997).
[48] X. Zheng *et al.* (Jefferson Lab Hall A Collaboration), Phys. Rev. C **70**, 065207 (2004).
[49] K. M. Kramer (Jefferson Lab E97-103 Collaboration), AIP Conf. Proc. **675**, 615 (2003).
[50] P. L. Anthony *et al.* (E155 Collaboration), Phys. Lett. B **553**, 18 (2003).
[51] A. Airapetian *et al.*, Eur. Phys. J. C **72**, 1921 (2012).
[52] D. Adams *et al.* (Spin Muon (SMC) Collaboration), Phys. Rev. D **56**, 5330 (1997).
[53] D. Stump, J. Pumplin, R. Brock, D. Casey, J. Huston, J. Kalk, H. L. Lai, and W. K. Tung, Phys. Rev. D **65**, 014012 (2001).
[54] F. James, Report No. CERN-D-506.
[55] A. Vogt, Comput. Phys. Commun. **170**, 65 (2005).
[56] M. Gluck, E. Reya, M. Stratmann, and W. Vogelsang, Phys. Rev. D **63**, 094005 (2001).
[57] J. Blumlein and H. Bottcher, Nucl. Phys. **B636**, 225 (2002).
[58] E. Leader, A. V. Sidorov, and D. B. Stamenov, Phys. Rev. D **73**, 034023 (2006).
[59] Y. Goto *et al.* (Asymmetry Analysis Collaboration), Phys. Rev. D **62**, 034017 (2000); M. Hirai, S. Kumano, and N. Saito (Asymmetry Analysis Collaboration), Phys. Rev. D **69**, 054021 (2004).
[60] D. de Florian, G. A. Navarro, and R. Sassot, Phys. Rev. D **71**, 094018 (2005).
[61] M. Botje, Eur. Phys. J. C **14**, 285 (2000).
[62] W. Furmanski and R. Petronzio, Z. Phys. C **11**, 293 (1982).
[63] S. A. Larin and J. A. M. Vermaseren, Phys. Lett. B **303**, 334 (1993).
[64] T. van Ritbergen, J. A. M. Vermaseren, and S. A. Larin, Phys. Lett. B **400**, 379 (1997).
[65] F. R. P. Bissey, V. A. Guzey, M. Strikman, and A. W. Thomas, Phys. Rev. C **65**, 064317 (2002).
[66] R. -W. Schulze and P. U. Sauer, Phys. Rev. C **48**, 38 (1993).
[67] R. W. Schulze and P. U. Sauer, Phys. Rev. C **56**, 2293 (1997).
[68] F. R. P. Bissey, A. W. Thomas, and I. R. Afnan, Phys. Rev. C **64**, 024004 (2001).
[69] I. Afnan, F. Bissey, J. Gomez, A. Katramatou, S. Liuti, W. Melnitchouk, G. Petratos, and A. Thomas, Phys. Rev. C **68**, 035201 (2003).
[70] S. Atashbar Tehrani and A. N. Khorramian, J. High Energy Phys. 07 (2007) 048.
[71] J. R. Ellis and R. L. Jaffe, Phys. Rev. D **9**, 1444 (1974) **10**, 1669(E) (1974).
[72] J. D. Bjorken, Phys. Rev. **148**, 1467 (1966).
[73] H. Burkhardt and W. N. Cottingham, Ann. Phys. (N.Y.) **56**, 453 (1970).
[74] R. L. Jaffe and X. D. Ji, Phys. Rev. D **43**, 724 (1991).
[75] X. Song, Phys. Rev. D **54**, 1955 (1996).
[76] M. Gockeler, R. Horsley, E. -M. Ilgenfritz, H. Perlt, P. E. L. Rakow, G. Schierholz, and A. Schiller, Phys. Rev. D **53**, 2317 (1996).
[77] R. L. Jaffe and X. Ji, Phys. Rev. D **43**, 724 (1991).
[78] F. M. Steffens, H. Holtmann, and A. W. Thomas, arXiv:hep-ph/9508398.
[79] E. Stein, P. Gornicki, L. Mankiewicz, A. Schafer, and W. Greiner, Phys. Lett. B **343**, 369 (1995).
[80] I. I. Balitsky, V. M. Braun, and A. V. Kolesnichenko, Phys. Lett. B **242**, 245 (1990) **318**, 648(E) (1993).
[81] S. E. Kuhn, J. P. Chen, and E. Leader, Prog. Part. Nucl. Phys. **63**, 1 (2009).
[82] S. A. Larin, T. van Ritbergen, and J. A. M. Vermaseren, Phys. Lett. B **404**, 153 (1997).
[83] A. V. Efremov, O. V. Teryaev, and E. Leader, Phys. Rev. D **55**, 4307 (1997).
[84] E. R. Nocera, S. Forte, G. Ridolf,i and J. Rojo, arXiv:1206.0201.